

# Spectropolarimetry of the WR + O Binary $\gamma^2$ Velorum during Periastron Passage

T. EVERSBERG,<sup>1</sup> A. F. J. MOFFAT,<sup>1,2</sup> AND S. V. MARCHENKO

Département de Physique, Université de Montréal, C.P. 6128, Succ. Centre Ville, Montréal, QC H3C 3J7, Canada; and Observatoire du Mont Mégantic; eversberg@astro.umontreal.ca, moffat@astro.umontreal.ca, sergey@astro.umontreal.ca

Received 1999 February 12; accepted 1999 April 1

**ABSTRACT.** We present low-resolution ( $\sim 6$  Å), high signal-to-noise spectropolarimetric observations obtained with the new William-Wehlau spectropolarimeter for the apparently brightest Wolf-Rayet star in the sky, the 78.5 day WR + O binary  $\gamma^2$  Velorum. Quasi-simultaneous monitoring of all four Stokes parameters  $I(\lambda)$ ,  $q(\lambda)$ ,  $u(\lambda)$ , and  $v(\lambda)$  was carried out over an interval of 31 nights centered on periastron. All emission lines in our observed wavelength interval (5200–6000 Å) show highly stochastic variations over the whole run. The phase-dependent behavior of the excess emission in the C III  $\lambda 5696$  line can be related to the wind-wind collision phenomenon. Varying features of Stokes  $q$  and  $u$  are seen across the strong lines, probably as a result of variable electron scattering of mainly continuum light. The spherical symmetry of the WR wind is thus broken by the presence of the O companion and clumping in the WR wind. Similar features in the extended red wing of the C III  $\lambda 5696$  emission line remain unexplained. No obvious circular line polarization features are seen across any emission line above the  $3\sigma \sim 0.03\%$  instrumental level.

## 1. INTRODUCTION

The object  $\gamma^2$  Velorum (WR 11 = HR 3207 = HD 68273; spectral type WC8 + O7.5–8 III–II) is the apparently brightest Wolf-Rayet (WR) star in the sky. It is a nearby binary system ( $d = 258^{+41}_{-31}$  pc; Schaerer, Schmutz, & Grenon 1997; van der Hucht et al. 1997) with an orbital period of 78.53 days (Schmutz et al. 1997, who also give a complete description of the orbit) and has the potential to represent a prototype of wind-wind interaction for massive stars with strong winds. Between the two stars the winds come to a complete stop at the stagnation point and material flows along a shock cone that wraps around the weaker wind O star (e.g., Stevens, Blondin, & Pollock 1992). The shock region, caused by collision at supersonic wind velocities, creates highly excited material that leads to excess emission via fast radiative cooling of the shocked gas (see, e.g., St-Louis, Willis, & Stevens 1993). Bartzakos (1998) used modified minimum spectra of the C III  $\lambda 5696$  line to estimate the collision excess in a number of short-period (2–16 day) WC + O binaries. For  $\gamma^2$  Vel, such a method has been slow in coming, probably because of its inconveniently long orbit and the presence of short-term stochastic multiscale struc-

tures in the C III  $\lambda 5696$  line of  $\gamma^2$  Vel (Lépine, Eversberg, & Moffat 1999). It was only after completing this project that we became aware of the spectroscopic study of Schweickhardt et al. (1999).

In this paper we concentrate on (1) the search for periodic line profile variations, following the contradictory reports of Jeffers, Stiff, & Weller (1985 and references therein) and Taylor (1990); (2) the behavior of the C III  $\lambda 5696$  line during periastron passage, in the anticipation that for WC stars this particular line should be the best indicator of a wind-wind collision in the optical (Bartzakos 1998); and (3) the search for any manifestation of a magnetic field and deviations from spherical symmetry in the WR wind.

The relatively long orbital period remains a practical handicap for a better understanding of  $\gamma^2$  Vel. For this reason we have attempted to answer some of these questions by observing prominent emission lines mainly around periastron passage, when the orbital configuration changes fastest.

## 2. OBSERVATIONS AND DATA REDUCTION

The star  $\gamma^2$  Vel was observed during a 5 week run in 1997 February/March with the William-Wehlau spectropolarimeter (Eversberg et al. 1998b) mounted on the 0.6 m telescope at the University of Toronto Southern Observatory (UTSO) on Las Campanas, Chile. We obtained spectra

<sup>1</sup> Visiting Astronomer, University of Toronto Southern Observatory, Las Campanas, Chile.

<sup>2</sup> Killam Research Fellow of the Canada Council for the Arts.

in all four wavelength-dependent Stokes parameters  $I$ ,  $Q/I \equiv q$ ,  $U/I \equiv u$ , and  $V/I \equiv v$  during 21 nights between February 18 and March 20 within  $\Delta\phi \sim \pm 0.2$  of periastron passage ( $\phi = 0.00$ ; O star in front at  $\phi = 0.03$ ; WR star in front at  $\phi = 0.61$ ). Individual spectra in  $I$  were obtained every  $\sim 3$  minutes, providing a typical signal-to-noise ratio of  $\sim 400 \text{ pixel}^{-1}$  in the continuum ( $\sim 600$  in the strong C III  $\lambda 5696$ , C IV  $\lambda 5806$  emission lines). Using the Garrison spectrograph (Garrison & Beattie 1990), the 3 pixel spectral resolution was about  $6 \text{ \AA}$  ( $\sim 320 \text{ km s}^{-1}$ ) in the wavelength range 5200–6000  $\text{\AA}$ , covering mainly the He II  $\lambda 5411$ , C IV  $\lambda 5471$ , C III  $\lambda 5696$ , C IV  $\lambda\lambda 5802, 5812$ , and He I  $\lambda 5875$  emission lines. Unfortunately, the data for nine nights (February 22–March 2) are of no use as a result of problems discovered later with the CCD readout.

As a consequence of the nonperfect behavior (as predictable for a fiber-fed system) of the polarimeter unit (see Eversberg et al. 1998b, who also give a detailed description of the data calibration procedure), we had to normalize the mean Stokes parameters  $q(\lambda)$ ,  $u(\lambda)$ , and  $v(\lambda)$  to zero, so that only relative line polarization could be obtained. This means that we were not able to estimate the degree and orientation of *broadband* polarization on the sky. Only relative line polarization and its variability were detectable.

### 3. RESULTS AND DISCUSSION

With our insufficient orbital coverage and low spectral resolution, we do not attempt to improve the orbital parameters. However, as a quick check we measured the central wavelengths of all prominent WR emission lines by fitting a single Gaussian profile.

Our velocity measurements for C IV  $\lambda 5471$  match best the predicted emission-line orbit (Schmutz et al. 1997). This is not surprising because this line is most Gaussian-like in form, unblended and well isolated. C IV  $\lambda\lambda 5802, 5812$  also fits fairly well, although this line is not of pure Gaussian form and is blended. All other moderately strong emission lines tend to follow the general shape of the orbital motion, but with increased amplitude. This increase is especially evident in He I  $\lambda 5876$  and, to a lesser extent, in C III  $\lambda 5696$  emission. This is primarily caused by the additional emission component changing its position on top of the underlying broad emission line as the stars go through periastron (see below).

Contributing  $\sim 80\%$  of the total continuum visual light (De Marco & Schmutz 1999), the O-star companion exhibits absorption lines mainly at He II  $\lambda 5411$ , O III  $\lambda 5592$ , and He I  $\lambda 5875$  in our spectra. Our relatively low spectral resolution does not allow a proper study of these lines, which in any case do not appear to show any significant variability in our spectra.

### 3.1. Stochastic Short-Term Variations

After co-adding all nightly spectra to yield a mean for each night and Doppler correcting them into the WR rest frame using the Schmutz et al. orbit, we co-added all nightly means to a global mean of the whole run. This global mean was then subtracted from the individual spectra in the WR frame, thus allowing us to study short-term ( $\sim$ hourly) variations. The resulting gray-scale plots of these residuals and the global mean are shown in Figures 1–3, for three consecutive intervals in orbital phase. In order to explore

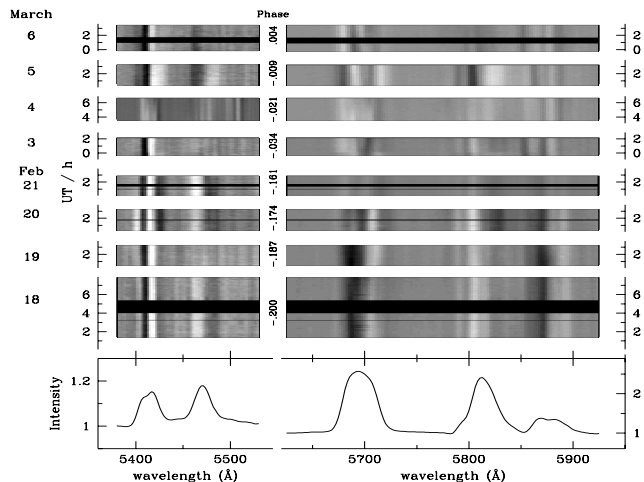


FIG. 1.—Observed spectra of  $\gamma^2$  Vel shifted to the WR frame for the nights of 1997 February 17/18–March 5/6. *Top*: Gray-scale plots of residuals from the mean rectified spectrum of the whole observing run plotted in time (stretched appropriately to fill in small time gaps) vs. wavelength. The gray-scale range is  $z = 0 \pm 0.1$  for the wavelengths 5380–5530  $\text{\AA}$  (left) and  $z = 0 \pm 0.2$  for the wavelengths 5620–5920  $\text{\AA}$  (right),  $z$  being the residual in continuum units. Different phases and respective UT dates and times are indicated. *Bottom*: Global (whole run) mean spectrum in the WR frame.

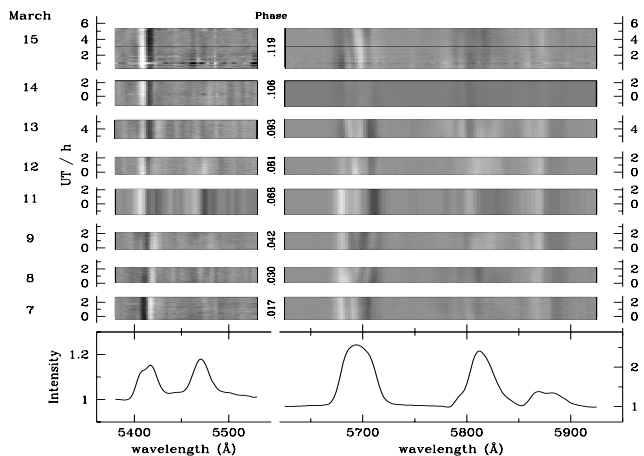


FIG. 2.—Same as Fig. 1 but for the nights 1997 March 6/7–14/15

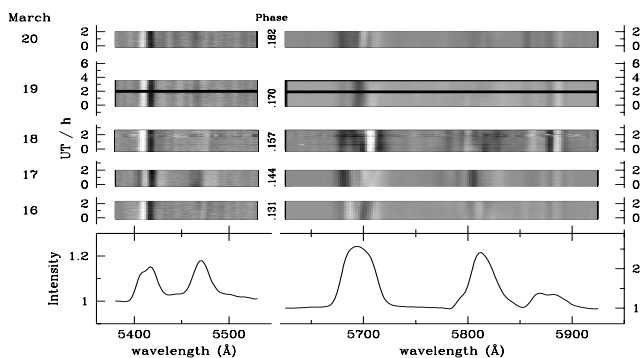


FIG. 3.—Same as Fig. 1 but for the nights 1997 March 15/16–19/20

the global variability, we calculate the standard deviation of pixel  $i$ :

$$\sigma_i = \sqrt{\frac{1}{n-1} \sum_{j=1}^n (I_{ij} - \bar{I}_i)^2}, \quad (1)$$

where  $I_{ij}$  is the rectified intensity of pixel  $i$  of the  $j$ th spectrum and  $\bar{I}_i$  is the global mean spectrum at pixel  $i$ . The results are shown in Figure 4 (*bottom*). Inspection of Figures 1–3 allows us to conclude the following:

1. C III  $\lambda 5696$ .—The most prominent nightly residuals are found in this line, which is already known to show stochastically emerging subpeaks with gradual motion away from the line center (Lépine et al. 1999: two-night high-resolution observations around phase  $\phi = 0.26$ –0.29).

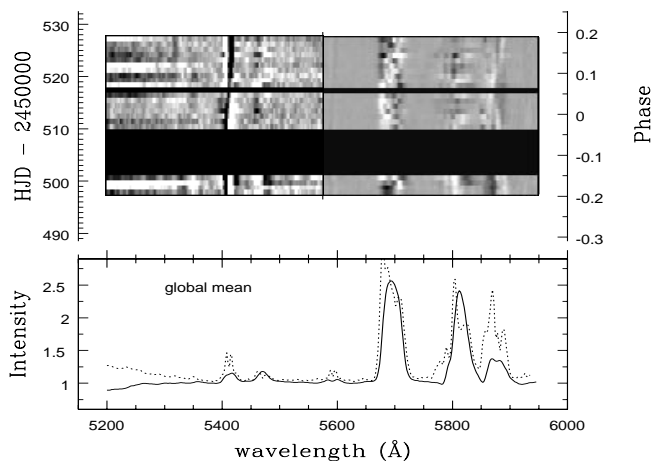


FIG. 4.—Long-term line variability. *Bottom*: Mean rectified spectrum (*solid line*) and standard deviation  $\sigma$  (*dashed line*) for the whole observing run in the WR frame. The  $\sigma$  profile is expanded by a factor 20 and shifted by 1 in intensity, to match the mean rectified line profile as closely as possible. *Top*: Gray-scale plot of residuals from the global mean rectified spectrum of each night plotted in time (stretched appropriately to fill in time gaps) vs. wavelength. The spectra have been Doppler corrected into the WR rest frame by using the orbit determined by Schmutz et al. (1997). The gray-scale range is  $z = 0 \pm 0.1$  for the wavelength interval 5200–5575 Å and  $z = 0 \pm 0.2$  for 5575–5950 Å.

Although our data are of lower resolution, we can confirm this kind of *stochastic* variability over a much longer timescale and far broader phase coverage. The movement of these subpeak features is well established in WR stars (e.g., Lépine 1998; Lépine & Moffat 1999) as well as in the O supergiant  $\zeta$  Puppis (Eversberg, Lépine, & Moffat 1998a) and interpreted as due to regions of higher density moving radially outward from the star and seen in projection in the line of sight.

2. C IV  $\lambda\lambda 5802, 5812$ .—In accordance with the idea of wind stratification (Kuhi 1973; Schulte-Ladbeck et al. 1995, and references therein), C IV  $\lambda\lambda 5802, 5812$  is assumed to be formed closer to the WR star than C III  $\lambda 5696$ . One might expect to detect stochastic variability in C IV  $\lambda\lambda 5802, 5812$  if the *whole* wind is structured. The variations are indeed detectable in C IV but are slightly smaller than in C III (Fig. 4). We find no clear correlation between the deviations in C III  $\lambda 5696$  and C IV  $\lambda\lambda 5802, 5812$ , partly because of the blended nature of the C IV line.

3. All the other three major observed emission lines are weaker, and the variability is sometimes close to the limit of detectability with our low spectral resolution. The two helium lines He II  $\lambda 5411$  and He I  $\lambda 5875$  are also affected by absorption of the O-star component. This absorption is easily detected in He II  $\lambda 5411$ , crossing the emission from blue to red during our run, in agreement with the predicted orbit. For He I  $\lambda 5875$  the O-component absorption is much less clear. A stochastic component of variability seems to dominate in this line, being loosely correlated with the variations in the C III  $\lambda 5696$  line. Variability in the C IV  $\lambda 5471$  line is also detectable but without sufficient quality to draw quantitative conclusions. Allowing for statistical fluctuations, the variation profile across the line,  $\sigma(\lambda)$  (Fig. 4, *bottom*), roughly follows the same basic shape of the line profile  $I(\lambda)$  itself, with  $\sigma(\lambda)/[I(\lambda) - I_c] \sim 5\%$  for C III  $\lambda 5696$ ,  $\sim 4\%$  for C IV  $\lambda\lambda 5802, 5812$ ,  $\sim 10\%$  for He II  $\lambda 5411$  and He I  $\lambda 5875$ , and  $\sim 3\%$  for C IV  $\lambda 5471$ . The effect of Poisson statistics for stronger lines is negligible ( $\lesssim 0.5\%$ ) compared with the intrinsic line variations.

### 3.2. Periodic Short-Term Variations

Do the observed emission lines show *periodic* variations on short timescales?

There are numerous, although controversial, reports about short-term variability in the spectrum of  $\gamma^2$  Vel, summarized in Jeffers et al. (1985): the profiles (or the line flux measured in the narrowband filters centered on prominent emission lines) show rapid, sometimes periodic variations on a typical timescale of 150–200 s. Far longer,  $P = 1.26$  hr and/or  $P = 2.0$  hr, coherent variations were discovered by Taylor (1990) in extensive narrowband photometric data

(He II  $\lambda 4686$  line and adjacent continuum) obtained at the South Pole.

Our data set allows us to search for periodic line profile variations in the relatively broad range, 6 minutes  $\leq P \leq 15$  days, on the high-quality spectra taken every  $\sim 3$  minutes over a typical interval of 2–3 hr in each of 21 nights during the 31 day run. Visual inspection of the individual spectra shows no apparent short-term ( $\sim$ minutes) variability. However, the spectra do vary on a much longer ( $\sim$ hours) timescale.

In order to search for a periodic component in the line profile variations, we have calculated power spectra (PS) using the technique of Scargle (1982). The raw PS were then reprocessed with the CLEAN algorithm in order to remove (reduce) the aliases and spurious features introduced by the unevenly spaced nature of the data (see Roberts, Lehár, & Dreher 1987). The calculations were performed for each wavelength pixel, using intensity readings in the spectra rebinned in a similar manner and Doppler corrected for orbital motion to the WR frame.

We started by analyzing individual nights, each consisting of 40–73 spectra. From here on we refer to the results obtained for the C III  $\lambda 5696$  emission line only (C IV  $\lambda \lambda 5802, 5812$  behaves similarly). We find no significant, periodic variations in the CLEANed PS over the  $50\text{--}75 \text{ day}^{-1} \leq \nu \leq 250 \text{ day}^{-1}$  frequency domain, with amplitudes exceeding the  $3 \sigma$  level of  $\sim 15\%$  of the line intensity. The nightly PS show some rise, roughly as  $\nu^{-1}$ , toward lower frequencies,  $\nu \leq 50\text{--}75 \text{ day}^{-1}$ , with typically three to five broad peaks slightly exceeding the  $3 \sigma$  level. We disregard these details as true indicators of periodic variations for two reasons: (1) the low-frequency structures are practically never repeated in consecutive nightly PS; (2) far more important, the peak structure is mimicked by the adjacent continuum. We know that the continuum is not involved in any *periodic* short-term activity (Taylor 1990). Thus, we interpret these low-frequency features as low-amplitude remnants of imperfectly CLEANed spectral windows, i.e., as artifacts arising from the uneven data sampling and finite lengths of the data records.

With no positive periodic detection in any of the nightly data sets, we combined the observations into blocks of three consecutive nights and repeated the analysis. The results are invariably negative, with no periods of  $A > 3 \sigma$  ( $\sim 6\%$  of the line intensity) for  $50\text{--}75 \text{ day}^{-1} \leq \nu \leq 250 \text{ day}^{-1}$ . There is some rise in the PS toward lower frequencies,  $\nu \leq 50\text{--}75 \text{ day}^{-1}$ , with broad peaks superposed on the  $\sim \nu^{-1}$  sloped PS. Even larger blocks of  $\sim$ week intervals bring the detectability limit down to  $A \leq 3\%$  of the line intensity, with no significant periodicity. The last step is to analyze the complete data set. For this we averaged the spectra of a given night into two to five group averages (depending on the level of variability and the number of spectra for the given night) and calculated the PS for the resulting 54 group

means. Again, there is no indication of significant periodicity in the  $0.07 \text{ day}^{-1} \leq \nu \leq 10 \text{ day}^{-1}$  frequency interval.

The only positive result we can infer from this exhaustive search is the  $\sim \nu^{-1}$  rise in the low-frequency part of the PS, probably indicating that we have detected aperiodic variations on timescales of  $\Delta t \geq 0.5$  hr.

### 3.3. Long-Term Variations

To monitor the phase-locked, long-term WR line variability through periastron passage, we created nightly mean residuals, plotting them in Figure 4. Significant long-term variations occur across the lines. All major lines but He II  $\lambda 5411$  show some excess variability on their blue flanks. This is not explainable by purely stochastic variability due to uniformly distributed clumps in a spherically symmetric wind but can be related to binary-induced effects (see § 3.4). The strong variations in the He II line are mainly due to the O-star absorption feature, clearly detected as moving across the line during our run and producing symmetric peaks in  $\sigma(\lambda)$  in Figure 4.

In Figure 5 we show the measured nightly averaged equivalent widths,  $W_\lambda$ , for the five prominent emission lines, corrected for the phase-dependent continuum variations of Marchenko et al. (1998b). As one can see, the C III  $\lambda 5696$

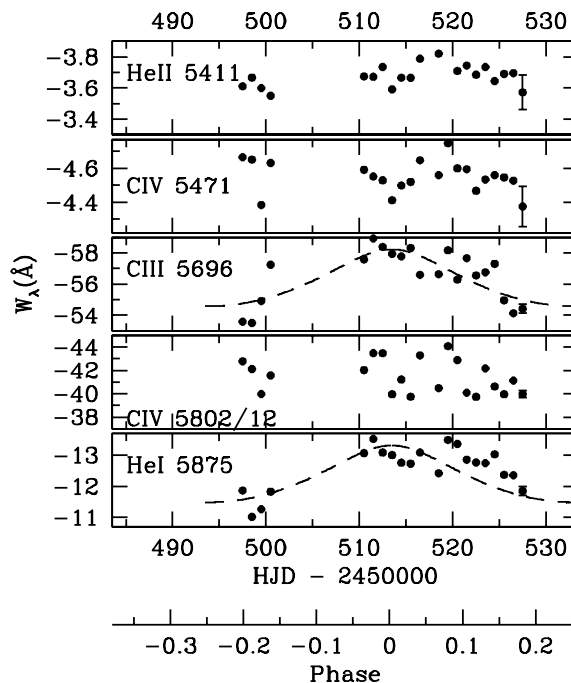


FIG. 5.—Equivalent widths of the nightly average emission lines, corrected for the phase-dependent continuum variations (Marchenko et al. 1998b). The typical  $2 \sigma$  errors estimated in accordance with Chalabaev & Maillard (1983) are indicated on the last data point of each plot. Dashed lines represent the relative inverse separation (arbitrary scale and zero point) between the two binary components.

and He I  $\lambda 5875$  line fluxes slightly increase before and then decrease after periastron passage with a maximum around closest approach, as was previously observed in C III  $\lambda 5696$  by St-Louis (1996). In contrast to C III and He I, the three other lines, all of higher ionization level, show no significant dependence on orbital phase. Additionally, there are large stochastic equivalent width variations in all prominent emission lines far exceeding the measurement errors. The phase-dependent changes in the C III  $\lambda 5696$  and He I  $\lambda 5875$  fluxes roughly follow a  $1/r$  dependence, where  $r$  is the orbital separation, as expected for the excess emission formed in the wind-wind collision zone (Stevens et al. 1992).

### 3.4. C III Excess

Although both He I  $\lambda 5875$  and C III  $\lambda 5696$  reveal similar phase-dependent long-term variations, here we concentrate on C III, since it is stronger and less blended than He I: the most recent attempts to quantify the O-star spectrum point to a O7.5–8 III–II spectral type (Schaerer et al. 1997; De Marco & Schmutz 1999), rejecting the previously suggested classification as a supergiant. For a typical O8 III star one may expect to see only weak, if any, emission at C III  $\lambda 5696$  (Walborn 1980), especially in view on the absence of any emission in the restored O-star H $\alpha$  profile (De Marco & Schmutz 1999). Neglecting the possibility of C III  $\lambda 5696$  emission from the O star, we may consider the C III  $\lambda 5696$  emission profile as consisting, in principal, of four different components: (1) emission from a constant, presumably spherically symmetric WR outflow (see below); (2) stochastic subfeatures due to clumping in the WR wind (Lépine 1998); and (3) phase-dependent excess emission created by colliding wind in a shock cone around the O star and (4) by heating of the WR wind by the O star. Effect 4 is seen even in some binaries with relatively large separation, e.g., the 21 day WN5+O binary WR 141 (Marchenko, Moffat, & Eenens 1998a). We do not consider WR atmospheric eclipses, as such are proved to be important in  $\gamma^2$  Vel (Schweickhardt et al. 1999) only around phases when the WR star is in front; these phases are not covered by our observations.

Disentangling these four components is a delicate problem, although successfully done for components 1 and 3 in several WR+O binaries (e.g., Marchenko et al. 1997; Moffat et al. 1998; Moffat, Marchenko, & Bartzakos 1996; Bartzakos 1998; Bartzakos, Moffat, & Niemela 1995). We have tried to distinguish between the excess emission and the globally spherically symmetric (however, locally clumpy) outflow under the following assumptions:

1. Emission arising from sources 3 and 4 is expected to be separation dependent, being weakest at apastron. This is indeed seen for  $\gamma^2$  Vel in Figure 5 as well as in the data of Schweickhardt et al. (1999). In this case the *minimum* inten-

sity spectrum in the WR frame over an extended observing run for a highly elliptical binary might represent the spherically symmetric WR outflow fairly well.

2. In the present data set, the largest projected separation between the two components occurs at  $\phi = \pm 0.2$ . In a zeroth approximation we use the actual minimum profile of the whole run as a representation (in reality an upper limit) of the spherical wind. We use this on  $\gamma^2$  Vel to test the shock-cone model developed by Lührs (1991, 1997).

Following this recipe, we Doppler corrected all the spectra of  $\gamma^2$  Vel into the WR rest frame and derived a global *minimum* spectrum. This minimum spectrum was then subtracted from the nightly mean spectra to obtain nightly excess emission spectra. The resulting gray-scale plot and the global minimum, mean, and maximum spectra of the whole run for the wavelength interval 5640–5940 Å are shown in Figure 6. As one can clearly see in Figure 6, excess emission above the minimum in C III  $\lambda 5696$  and, less clearly, He I  $\lambda 5875$  is phase dependent. This feature moves from the red to the blue line flank and back during the run. This excess emission causes large deviations in the RV curves of He I  $\lambda 5875$  and C III  $\lambda 5696$  from the “normal” orbital motion, as mentioned above.

Lührs (1991, 1997) has developed a simple model to describe the phase-dependent variations of the excess emission in WR+O binaries with *circular* orbits. Assuming optically thin emission from a hot plasma wrapping around the O-star component and moving with velocity  $v_s$  along a cone with opening half-angle  $\Theta$ , deflected in the orbital

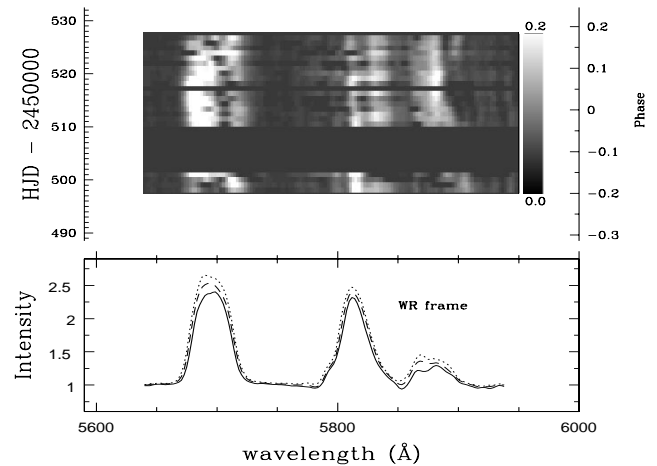


FIG. 6.—Nightly excess emission spectra above the minimum level. *Bottom*: Global minimum (solid line), mean (dashed line), and maximum (dotted line) profile for the whole observing run in the WR frame. *Top*: Gray-scale plot of residuals from the global minimum spectrum of each night plotted in time (stretched appropriately to fill in time gaps) vs. wavelength. The spectra have been Doppler corrected to the WR frame by using the orbit determined by Schmutz et al. (1997). The gray scale ranges over  $z = 0-0.2$ , as indicated on the right.

plane by an angle  $\delta\phi$  due to the Coriolis effect associated with orbital motion, one finds (see also Moffat et al. 1998) that the double-peak excess emission from the cone has an average velocity  $\bar{v}$  and peak-to-peak width  $2v_*$  of

$$\bar{v} = v_s \cos \Theta \sin i \cos(\phi - \delta\phi), \quad (2)$$

$$2v_* = 2v_s \sin \Theta \sqrt{1 - \sin^2 i \cos^2(\phi - \delta\phi)}, \quad (3)$$

with  $\phi$  the orbital phase  $\in \{0, 2\pi\}$  and  $i$  the inclination. For the analysis of  $\gamma^2$  Vel with an eccentric orbit we follow Moffat et al. (1998), by replacing  $\phi$  by  $w + \omega - \pi/2$  and  $\delta\phi$  by  $\delta w$ , with  $w$  the true anomaly and  $\omega$  the usual periastron angle:

$$\bar{v} = v_s \cos \Theta \cos(w + \omega - \delta w - \pi/2), \quad (4)$$

$$2v_* = 2v_s \sin \Theta \sqrt{1 - \sin^2 i \cos^2(w + \omega - \delta w - \pi/2)}. \quad (5)$$

In our situation with the high intrinsic noise level of the variations and the uncertainty in the appropriate template profile to extract the excess emission,  $\bar{v}$  and  $2v_*$  are not clearly defined. For this reason we calculated a more robust value of a weighted average line-of-sight (LOS) velocity  $\bar{v}$  with

$$\bar{v} = \frac{\sum_i I_i v_i}{\sum_i I_i} \quad (6)$$

and a weighted average width  $2\sigma$  to characterize the peak separation, adding a constant  $2v_c$ :

$$2v_* \rightarrow 2\sigma + 2v_c = 2 \sqrt{\frac{\sum_i I_i (v_i - \bar{v})^2}{\sum_i I_i}} + 2v_c, \quad (7)$$

with  $v_i$  the LOS velocity and  $I_i$  the residual line intensity at pixel  $i$ . The newly introduced constant  $2v_c$  reflects the fact that the bow-shock emission is likely to be significantly broadened as a result of large-scale turbulence (Walder & Folini 1998) in the wind-wind collision zone.

To test our procedure we also created a true minimum and various smoothed (boxcar of 3, 5, 7 and 9 pixels) minimum spectra from the  $\gamma^2$  Vel data and a minimum template from the smoothed C III line of WR 135 (data from Lépine & Moffat 1999). The latter template was produced by normalizing the C III line of WR 135 in height and width to C III in  $\gamma^2$  Vel via simple comparison of its lower, less variable part. Note that WR 135 has the same subtype and even wind terminal velocity as the WR component in  $\gamma^2$  Vel. Smoothing of the minimum spectra of  $\gamma^2$  Vel does not significantly change the output results. However, the WR 135

template was found to be unsatisfactory, due to the subtle differences in the uppermost parts of the profiles. Thus, we retain the true minimum (no smoothing) profile of  $\gamma^2$  Vel in our modeling (Fig. 7). As we face the serious problem of the unknown true minimum spectrum, with the additional complication from the presence of large stochastic line variations, we are not able to perform a quantitatively meaningful multiparametric fit to find the values of  $v_c$ ,  $v_s$ ,  $\theta$ ,  $\delta w$ , and  $i$ . Instead, whenever possible, we use known or otherwise reasonable values for these parameters.

The short-dashed and long-dashed lines in Figure 7 show the predictions of the Lührs model for two values of  $\delta w$ . Willis, Schild, & Stevens (1995) estimated  $\Theta \sim 25^\circ$  from their *ROSAT* X-ray observations. In fact, the opening angle might be at least a factor of 2 larger, judging by the appearance of the O-star high-velocity absorption  $\sim 0.09$  in phase before periastron passage (St-Louis et al. 1993). Also, the revised  $\dot{M}$  of the WR star [ $\dot{M} = (0.7-3.0) \times 10^{-5}$ ; Schmutz et al. 1997; Schaerer et al. 1997; Nugis, Crowther, & Willis 1998] leads to  $\Theta = 45^\circ-68^\circ$ , using the formalism from Eichler & Usov (1993) and Canto, Raga, & Wilkin (1996).

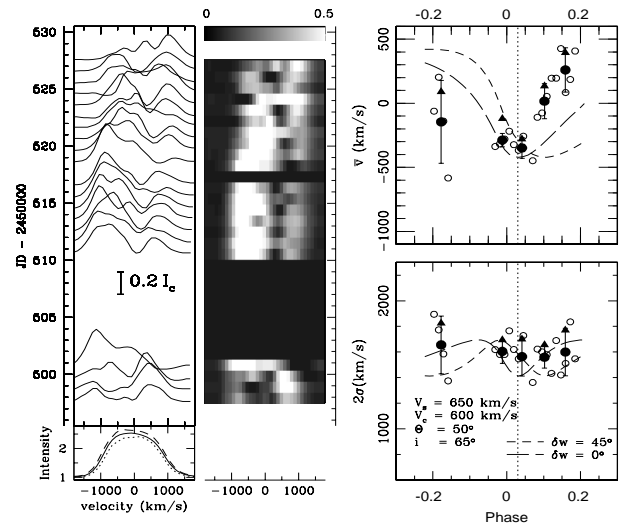


FIG. 7.—Extracted C III  $\lambda 45696$  excess emission spectra of  $\gamma^2$  Vel for different orbital positions in the observer's frame. *Top left*: Intensity plot of nightly residuals from the minimum spectrum of the whole observing run plotted in time vs. LOS velocity. *Bottom left*: Global maximum (long-dashed line), mean (solid line), and minimum (dotted line) line profile of C III  $\lambda 45696$ . *Center*: Gray-scale plot of nightly residuals from the minimum line profile plotted in time (stretched appropriately to fill in time gaps) vs. LOS velocity. The gray-scale range is  $z = 0-0.2$ . *Right*: Comparison of the observed average velocities (*top*) and line widths (*bottom*) of the excess emission with the Lührs model. *Open circles*: Excess using the global minimum for each night. *Filled circles*: Average excess emission of four-night bins ( $2\sigma$  error bars are indicated). *Filled triangles*: Average excess emission of four-night bins including backscattered light. The vertical dotted lines indicate the position when the O star is in front of the WR component. The short-dashed curves represent the theoretical calculation using the Lührs model with  $\delta w = 45^\circ$ ; the long-dashed curves are for  $\delta w = 0^\circ$ .

The latter value of  $\Theta$  must be treated as an upper limit because of the reclassification of the O component from O9 I to O8 III (Schaerer et al. 1997), with potential diminishing of  $\dot{M}$ (O star). We assume that the Coriolis deflection  $\delta w$  lies somewhere between  $0^\circ$  and  $45^\circ$ , judging by the phase dependence of the X-ray flux. First, we fix the stream velocity,  $v_s = 650 \text{ km s}^{-1}$ , the cone-opening half-angle  $\Theta = 25^\circ$  (Stevens et al. 1996),  $i = 65^\circ$ , and two different values of the Coriolis deflection,  $\delta w = 0^\circ$  (*long-dashed line*) and  $\delta w = 45^\circ$  (*short-dashed line*). Note that the model is not very sensitive to the choice of  $i$  within the proposed range  $i = 65^\circ \pm 8^\circ$  (Schmutz et al. 1997). This leaves us with the only unaccounted for free parameter  $2v_c$ . Formally chosen as  $2v_c \sim 2\sigma_{\text{turbulent}}$  (up to  $400 \text{ km s}^{-1}$  in  $\gamma^2$  Vel: Lépine et al. 1999), it does not apply in practice to the observational data. Obviously, this parameter is heavily biased by the subtraction of a probably inadequate template. Because of the nature of this bias, we expect  $2v_c$  to be somewhere between  $2v_{\text{turbulent}} \sim 400 \text{ km s}^{-1}$  and  $2v_{\text{shock}} \cong 2300\text{--}2600 \text{ km s}^{-1}$  (twice the velocity of the WR wind entering the wind-wind collision zone; see St-Louis et al. 1993). Indeed, we find  $2v_c = 1200 \text{ km s}^{-1}$  as a reasonable compromise to match the data.

With the above parameters we find that the modeled variations in  $\bar{v}$  far exceed the observed amplitude. This can be counteracted by increasing the opening angle  $\Theta$ . This additionally affects  $\delta w$ , requiring  $\delta w \ll 45^\circ$ . The possibility of increasing  $\Theta$  is related to the revised  $\dot{M}$ (WR), as mentioned before, and also to the strong wind braking effect (sudden deceleration of the WR wind by the O-star radiation just before it enters the bow-shock zone) predicted for this system (Gayley, Owocki, & Cranmer 1997). We therefore change  $\Theta$  from  $25^\circ$  to  $50^\circ$ , taking this as a tentative estimate. The change brings the calculated  $\bar{v}$  much closer to the data.

However, despite the qualitative similarity of the observed and modeled  $\bar{v}$  curves, there are large systematic deviations. The first reason for this might be the unaccounted presence of light from the O star backscattered off the WR wind, especially important around periastron passage. We include this process in our model, however rather schematically, approximating the scattered light by a Gaussian profile of fixed central intensity and half-width. We also allow for the Doppler shift of this component in accordance with the orbital motion as well as a  $\delta w = 45^\circ$  phase deflection (as an upper limit of the redistributed flux). This deflection is based on the consideration of overheating of the O-star surface by the X-ray flux coming from the bow-shock head (see Gies, Bagnuolo, & Penny 1997). Yet another potential source of deviation between observed and modeled  $\bar{v}$  curves may arise from the absorption-like feature which appears to cross the excess emission from red to blue around JD 2,450,525. We have no explanation for this feature.

Inclusion of backscattered light does not remove the disparity between the modeled and observed  $\bar{v}$ . We have no feasible explanation for these deviations. However, we can conclude that the backscattered light plays a relatively minor role in the observed phase-related line-profile variations. We share this conclusion with St-Louis et al. (1993). Considering the number of assumptions required to obtain the minimum C III profile, along with the strong profile variations unrelated to the wind-wind collision, our model provides only a qualitative indication that the wind-wind collision is likely at work in this system.

Some support for our results comes from an independent study. Recent analysis of optical line emission and its variability in  $\gamma^2$  Vel has been carried out by Schweickhardt et al. (1999). By comparing their data from an extended observing run with a model for occultation effects developed by Auer & Koenigsberger (1994), they conclude that the observed line profile variability around periastron passage in C III  $\lambda 4650$  (partly blended with C IV  $\lambda 4658$ ) cannot be explained by occultation. They therefore state that the excess C III  $\lambda 4650$  emission arises, at least partly, from wind-wind collision in  $\gamma^2$  Vel.

The most interesting detail readily seen in Figure 2 of Schweickhardt et al. (1999) is the swift change, by as much as  $1000 \text{ km s}^{-1}$ , of the velocity of the excess emission in C III  $\lambda 4650$  at  $\phi$  between  $-0.15$  and  $-0.10$ . This is confirmed by our observations in Figure 7, where one sees a  $\sim 500 \text{ km s}^{-1}$  jump in  $\bar{v}$  for C III  $\lambda 5696$  at  $\phi \sim -0.15$ . This phenomenon repeats over many orbital cycles; hence, we discard stochastic wind variability as a cause. We note that around periastron passage, the changing wind momentum balance (see Gayley et al. 1997) may provoke crashing of the WR wind onto the O-star surface. This may significantly change the mass load into the wind-wind collision zone as well as its geometry (phase-variable  $\Theta$  and reduced  $\delta w$ ) and physical conditions, increasing the emissivity from the wind-wind collision component (note the rise in  $W_\lambda$  of He I and C III in Fig. 5), thus creating much stronger extra blueshifted emission, and, finally, shifting the WR profile to negative velocities. It is relevant to note that the wind velocity of the O star tends to be lower during periastron passage (Stevens et al. 1996), which might signify an abrupt change in the dynamics of the wind-wind collision process.

Another detail to be mentioned is the pronounced asymmetry between the ingress-egress behavior of the excess emission, suggestive of more gradual liftoff of the shock from the O-star surface after the initial swift crushing. This asymmetry is probably created by the orbital motion of the components, in direct analogy to another highly eccentric colliding-wind binary,  $\iota$  Orionis (Pittard 1998).

Now we are able to explain the excess variability in the blue wing of the carbon and He I lines in Figure 4. According to the Lührs model with allowance for crashing of the WR wind onto the O star, strong excess emission is

expected to shift to the blue when the O star is approximately in front, i.e., around periastron passage. This introduces larger values for the scatter  $\sigma$  in the blue wing of our data. This is clearly detected in all the five strong emission lines, except He II  $\lambda 5411$ , where the excess emission is masked by the strong O-star absorption.

### 3.5. Polarization

The shock cone introduces a deviation from spherical symmetry in the WR wind so that, in principle, it could lead to phase-dependent intrinsic continuum polarization. However, an even more important source of phase-dependent *continuum* polarization is the scatter of O-star light off free electrons in the WR wind (see St-Louis et al. 1987 for  $\gamma^2$  Vel and other WC+O binaries). On the other hand, *WR emission-line* flux in a binary will be practically unpolarized. This might cause some phase-dependent variations of polarization occurring at the positions of the emission lines (see Moffat & Piirola 1994). In general, a flattened WR wind can also cause some line depolarization (see Harries, Hillier, & Howarth 1998), which however is not expected to vary with phase in a binary system.

To obtain sufficient accuracy in  $q$ ,  $u$ , and  $v$  we co-added all nightly Stokes parameters, Doppler corrected into the WR rest frame to provide global mean Stokes  $q$ ,  $u$ , and  $v$  spectra for the whole run, consisting of  $\sim 80$  hr of exposure time in total. The result is shown in Figure 8.

We draw attention in Figure 8 to the depressions ( $\sim 0.05\%$ ) in Stokes  $q$  and  $u$  across the two strong lines of C III  $\lambda 5696$  and C IV  $\lambda\lambda 5802, 5812$ , significantly above the  $3\sigma$  noise level,  $\sim 0.03\%$ . We calculate this precision limit from the featureless  $v(\lambda)$  spectrum between 5600 and 5950  $\text{\AA}$ .<sup>3</sup> The He I  $\lambda 5875$  line also shows complex structure, although closer to the noise limit. Phase-locked  $q$ ,  $u$  variations in the continuum light, clearly seen around periastron passage in broadband polarization (St-Louis et al. 1987), have probably diluted the line polarization effect, which for  $q$  and  $u$  is expected to be the largest at quadratures. Additionally, any regular variations across the line profiles are masked by omnipresence of the strong stochastic component. Thus, if there are any phase-related variations in the Stokes spectra, our data do not reveal them.

We find no significant circular polarization along the whole mean  $v_\lambda$  spectrum, in excess of the instrumental level of  $3\sigma \sim 0.03\%$ , although there are hints of variability at the blue edges of C III  $\lambda 5696$ , C IV  $\lambda\lambda 5802, 5812$ , and He I  $\lambda 5876$ . The technique of magnetic field measurement has been

<sup>3</sup> We define the noise of pixel  $i$  as  $\sigma_i/\sqrt{N}$ , with the  $\sigma_i$  as defined in eq. (1) and  $N$  as the number of rectified polarization spectra. We assume that the  $v(\lambda)$  spectrum is entirely noise dominated. The photon statistics and observation technique are identical in  $q$ ,  $u$ , and  $v$ .

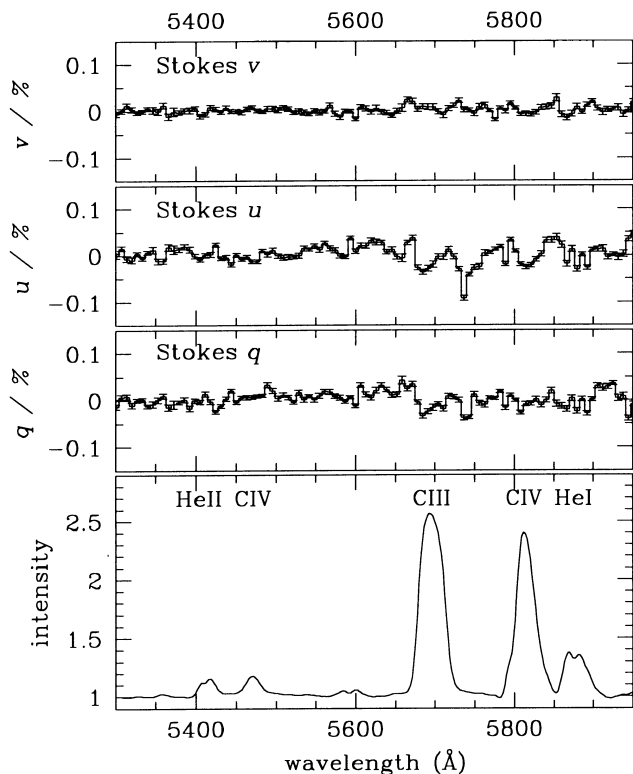


FIG. 8.—Mean rectified intensity spectrum (*bottom*) and mean Stokes  $q$ ,  $u$ , and  $v$  (*top*) for the whole observing run in the WR frame. The polarimetric data have been binned by a 5 pixel boxcar. Formal  $2\sigma$  error bars are indicated.

described by Landstreet & Borra (1977a, 1977b), Borra & Landstreet (1980), and Landstreet (1977, 1982). Landstreet followed Unno (1956) by using the Milne-Eddington approximation for the source function with presence of polarized light. For this case he derived

$$\langle v \rangle = 4.67 \times 10^{-13} z B_e \lambda^2 (dI/d\lambda) / I, \quad (8)$$

with  $\langle v \rangle = (v_{\text{red}} - v_{\text{blue}})/2$ , where  $v_{\text{red}}$  and  $v_{\text{blue}}$  are the fractional polarizations in the red and blue line wings, respectively,  $z$  is the Landé factor, and  $B_e$  is the net effective longitudinal component of the magnetic field in units of gauss. In our case we have no recognizable differences between  $v_{\text{red}}$  and  $v_{\text{blue}}$ . For this reason we take  $\langle v \rangle \leq 0.03\%$  (our calculated noise level).

Instead of estimating a magnetic field strength in an absorption-line star with a visible photosphere, we use this equation for the emission lines from the extended wind in  $\gamma^2$  Vel. By using equation (8) we ignore the Doppler shifts experienced by flux coming from different parts of the stellar wind. On the other hand Mathys (1999) points out that equation (8) requires a correction factor of  $\frac{4}{3}$  to be applicable for emission-line stars. By using equation (8) and this correction with the Landé factor  $z = 1$  for this tran-

sition ( $3^1P^0 - 3^1D$ ), the slope of the line flanks, and the central line intensity of C III  $\lambda 5696$ , we translate the instrumental noise level into an upper limit on the net effective magnetic field in  $\gamma^2$  Vel:  $B_e \leq 280$  G.

#### 4. SUMMARY

We have presented phase-dependent spectropolarimetry for the WR+O binary  $\gamma^2$  Vel, obtained with the new William-Wehlau spectropolarimeter. In the wavelength range 5200–6000 Å this includes the dominant lines of He II  $\lambda 5411$ , C IV  $\lambda 5471$ , C III  $\lambda 5696$ , C IV  $\lambda \lambda 5802, 5812$ , and He I  $\lambda 5875$ . All four Stokes parameters  $I$ ,  $q$ ,  $u$ , and  $v$  have been obtained quasi-simultaneously during an extended run through periastron passage ( $\phi = -0.2$  to  $0.2$ ). We note the following:

1. All five observed major emission lines show small-scale peaks over the broad underlying emission profiles, stochastically changing from night to night and in some nights moving toward the blue/red line wings. These sub-peaks are assumed to be a manifestation of localized high-density regions (clumps, blobs) created by radiative instabilities (Owocki 1994), outwardly propagating in the wind (see Lépine 1998). Their presence in lines of different ionization implies that the whole wind is affected by clumping.

2. Measurements of the line equivalent widths also show significant stochastic variability in the stronger lines of C III  $\lambda 5696$ , C IV  $\lambda \lambda 5802, 5812$ , and He I  $\lambda 5875$ .

3. The variation profiles across the lines,  $\sigma(\lambda)$ , roughly follow the shape of the emission-line profiles themselves, with  $\sigma_\lambda/(I_\lambda - I_c) \sim 3\% - 10\%$ , depending on the line. This

indicates that the whole wind is affected by stochastic variations.

4. We find no evidence for a coherent periodic component in the line profile variations of  $\gamma^2$  Vel, from  $\sim 6$  minutes to 15 days.

5. We make an attempt to disentangle the components of the phase-dependent, variable emission under certain assumptions. This reveals some interesting wind-wind collision effects, with a hint of crashing of the WR wind onto the O star during periastron passage.

6. We report a weak depolarization effect across the strong emission lines of C III  $\lambda 5696$  and C IV  $\lambda \lambda 5802, 5812$ , which could be related to the phase-dependent asymmetry created by the O-star light scattered off by free electrons in the WR wind (Moffat & Piirola 1994).

7. No definite circular polarization is detected in the emission lines above the instrumental  $3\sigma$  threshold of 0.03%, placing an upper limit on the net effective magnetic field in the WR wind:  $B_e \leq 280$  G.

The authors would like to thank Bob Garrison for the generous allotment of observing time at UTSO, Steve Steeles for his continuous support during the observations at UTSO, and Doug Gies for helpful suggestions. T. E. is grateful for full financial aid from the Evangelisches Studienwerk/Germany, which is supported by the German government, as well as an extended bursary from the astronomy group at the Université de Montréal. A. F. J. M. thanks NSERC (Canada), FCAR (Québec), and the Killam program of the Canada Council for the Arts for financial support.

#### REFERENCES

- Auer, L. H., & Koenigsberger, G. 1994, *ApJ*, 436, 869  
 Bartzakos, P. 1998, doctoral thesis, Univ. Montréal  
 Bartzakos, P., Moffat, A. F. J., & Niemela, V. S. 1995, in *IAU Symp. 163, Wolf-Rayet Stars: Binaries, Colliding Winds, Evolution*, ed. K. A. van der Hucht & P. M. Williams (Dordrecht: Kluwer), 406  
 Borra, E. F., & Landstreet, J. D. 1980, *ApJ*, 212, 141  
 Cantó, J., Raga, A. C., & Wilkin, F. P. 1996, *ApJ*, 469, 729  
 Chalabaev, A., & Maillard, J. P. 1983, *A&A*, 127, 279  
 De Marco, O., & Schmutz, W. 1999, *A&A*, 345, 163  
 Eichler, D., & Usov, V. 1993, *ApJ*, 402, 271  
 Eversberg, T., Lépine, S., & Moffat, A. F. J. 1998a, *ApJ*, 494, 799  
 Eversberg, T., Moffat, A. F. J., Debruyne, M., Rice, J., Piskunov, N., Bastien, P., Wehlau, W. H., & Chesneau, O. 1998b, *PASP*, 110, 1356  
 Garrison, R. F., & Beattie, B. 1990, *JRASC*, 84, 246  
 Gayley, K. G., Owocki, S. P., & Cranmer, S. R. 1997, *ApJ*, 475, 786  
 Gies, D. R., Bagnuolo, W. G., Jr., & Penny, L. R. 1997, *ApJ*, 479, 408  
 Harries, T. J., Hillier, D. J., & Howarth, I. D. 1998, *MNRAS*, 296, 1072  
 Jeffers, S., Stiff, T., & Weller, W. G. 1985, *AJ*, 90, 1852  
 Kuhl, L. V. 1973, *ApJ*, 180, 783  
 Landstreet, J. D. 1977, *AJ*, 85, 611  
 ———. 1982, *ApJ*, 258, 639  
 Landstreet, J. D., & Borra, E. F. 1977a, *ApJ*, 212, L43  
 ———. 1977b, *ApJ*, 224, L5  
 Lépine, S. 1998, Ph.D. thesis, Univ. Montréal  
 Lépine, S., Eversberg, T., & Moffat, A. F. J. 1999, *AJ*, 117, 1441  
 Lépine, S., & Moffat, A. F. J. 1999, *ApJ*, 514, 909  
 Lührs, S. 1991, doctoral thesis, Univ. Münster  
 ———. 1997, *PASP*, 109, 504  
 Marchenko, S. V., Moffat, A. F. J., & Eenens, P. R. J. 1998a, *PASP*, 110, 1416  
 Marchenko, S. V., Moffat, A. F. J., Eenens, P. R. J., Cardona, O., Echevarria, J., & Hervieux, Y. 1997, *ApJ*, 485, 826  
 Marchenko, S. V., et al. 1998b, *A&A*, 331, 1022  
 Mathys, G. 1999, in *IAU Colloq. 169, Variable and Non-spherical Stellar Winds in Luminous Hot Stars*, ed. B. Wolf, A. W. Fullerton, & O. Stahl, in press  
 Moffat, A. F. J., Marchenko, S. V., & Bartzakos, P. 1996, *Rev. Mexicana Astron. Astrofis. Conf. Ser.*, 5, 38

- Moffat, A. F. J., & Piirola, V. 1994, *ApJ*, 413, 724  
Moffat, A. F. J., et al. 1998, *ApJ*, 497, 896  
Nugis, T., Crowther, P. A., & Willis, A. J. 1998, *A&A*, 333, 956  
Owocki, S. P. 1994, *Ap&SS*, 221, 3  
Pittard, J. M. 1998, *MNRAS*, 300, 479  
Roberts, D. H., Lehár, J., & Dreher, J. W. 1987, *AJ*, 93, 968  
Scargle, J. D. 1982, *ApJ*, 263, 835  
Schaerer, D., Schmutz, W., & Grenon, M. 1997, *ApJ*, 484, L153  
Schmutz, W., et al. 1997, *A&A*, 328, 219  
Schulte-Ladbeck, R. E., Eenens, P. R. J., & Davis, K. 1995, *ApJ*, 454, 917  
Schweickhardt, J., Kaufer, A., Schmutz, W., Stahl, O., & Wolf, B. 1999, in *IAU Colloq. 169, Variable and Non-spherical Stellar Winds in Luminous Hot Stars*, ed. B. Wolf, A. W. Fullerton, & O. Stahl, in press  
Stevens, I. R., Blondin, J. M., & Pollock, A. M. T. 1992, *ApJ*, 386, 265  
Stevens, I. R., Corcoran, M. F., Willis, A. J., Skinner, S. L., Pollock, A. M. T., Nagase, F., & Koyama, K. 1996, *MNRAS*, 283, 589  
St-Louis, N. 1996, *Rev. Mexicana Astron. Astrofis. Conf. Ser.*, 5, 76  
St-Louis, N., Drissen, L., Moffat, A. F. J., Bastien, P., & Tapia, S. 1987, *ApJ*, 322, 870  
St-Louis, N., Willis, A. J., & Stevens, I. R. 1993, *ApJ*, 415, 298  
Taylor, M. 1990, *AJ*, 100, 1264  
Unno, W. 1956, *PASJ*, 8, 108  
van der Hucht, et al. 1997, *NewA*, 2, 245  
Walborn, R. N. 1980, *ApJS*, 44, 535  
Walder, R., & Folini, D. 1998, *A&A*, 330, L21  
Willis, A. J., Schild, H., & Stevens, I. R. 1995, *A&A*, 298, 549